Radio Science, Volume 36, Number 1, Pages 107–117, January–February 2001

Reliability analysis in aperture synthesis interferometric radiometers: Application to *L* band Microwave Imaging Radiometer with Aperture Synthesis instrument

M. Vall-llossera, N. Duffo, A. Camps, I. Corbella, F. Torres and J. Bará
Universitat Politècnica de Catalunya, Barcelona, Spain

Abstract. The Microwave Imaging Radiometer with Aperture Synthesis (MIRAS) instrument will be the first radiometer using aperture synthesis techniques for Earth observation. It will be boarded in the Soil Moisture and Ocean Salinity (SMOS) Earth Explorer Opportunity Mission of the European Space Agency and launched in 2005. The configuration under study in the MIRAS Demonstrator Pilot Project is a Y-shaped array with 27 dual-polarization *L* band antennas in each arm, spaced 0.89 wavelengths. In addition to these 81 antennas there are 3 additional ones between the arms for phase restoration and redundancy purposes and an extra one at the center of the Y array that is connected to a noise injection radiometer. The digitized in-phase and quadrature outputs of each receiver are multiplexed in groups of four and optically transmitted to the hub where the complex cross correlations are computed. In this configuration there are 85 antennas-receiving channels and 21 multiplexers. The objectives of this paper are twofold: (1) the study of the performance degradation of Y-shaped aperture synthesis interferometric radiometers in case of single or multiple subsystem failures and (2) a reliability analysis at subsystem level.

1. Introduction to Aperture Synthesis Interferometric Radiometers

1.1. Principles of Operation

The basic measurement of an aperture synthesis interferometric radiometer is the visibility function Vkl, in units of Kelvin, obtained from the complex cross correlation of the signals $b_k(t)$ and $b_l(t)$ measured by every pair of antennas denoted k and l (Figure 1). The antennas are located above the XY plane in positions $(x_{k,l}, y_{k,l})$ forming the baseline $(u_{kl}, v_{kl}) = (x_l - x_k, y_l - y_k)/\lambda_0$ [*Thompson et al., 1986; Ruf et al., 1988*]. The sample of the visibility function at this baseline is given by

$$V_{kl} = V(u_{kl}, v_{kl}) \stackrel{\Delta}{=} \frac{1}{k_B\sqrt{B_k B_l}\sqrt{G_k G_l}} \frac{1}{2}\left\langle b_k(t) b_l^*(t)\right\rangle$$

$$\stackrel{\Delta}{=} \frac{1}{\sqrt{\Omega_k \Omega_l}} \iint_{\xi^2+\eta^2\le 1} \frac{T_B(\xi,\eta)}{\sqrt{1-\xi^2-\eta^2}} F_{nk}(\xi,\eta) F_{nl}^*(\xi,\eta)$$

$$\tilde{r}_{kl}\left(-\frac{u_{kl}\xi + v_{kl}\eta}{f_0}\right) \exp\left[-j2\pi(u_{kl}\xi + v_{kl}\eta)\right] d\xi d\eta, \qquad (1)$$

Paper number 2000RS002514.
0048-6604/01/2000RS002514$11.00

where k_B is the Boltzmann constant, $B_{k,l}$ and $G_{k,l}$ are the noise bandwidth and the power gain of the receiving chains, $\Omega k,l$ and $F_{nk,l}(\xi,\eta)$ are the equivalent solid angle and the normalized radiation voltage patterns of the antennas, assumed to be located over the XY plane, and < > stands for the time average operator. The directional cosines $(\xi,\eta) = (\sin\theta\cos\phi, \sin\theta\sin\phi)$ are defined with respect to the X and Y axes respectively (Figure 1), and is the so-called fringe-wash function, which accounts for spatial decorrelation effects and depends on the normalized frequency response $H_{nk,l}(f)$ of each channel [*Camps et al.*, 1999]. In the ideal case (identical antennas and receivers and negligible spatial decorrelation effects) the relationship between the visibility samples and the brightness temperature image (weighted by the antenna pattern and the obliquity factor $(1-\xi^2-\eta^2)^{-1/2}$ is simply a Fourier transform.

1.2. Configuration of the Microwave Imaging Radiometer With Aperture Synthesis (MIRAS) Instrument

MIRAS makes use of hexagonal sampling of the (u,v) spatial frequency plane which minimizes the associated electronics. The antennas are uniformly spaced $d = 0.89$ wavelengths along three arms forming

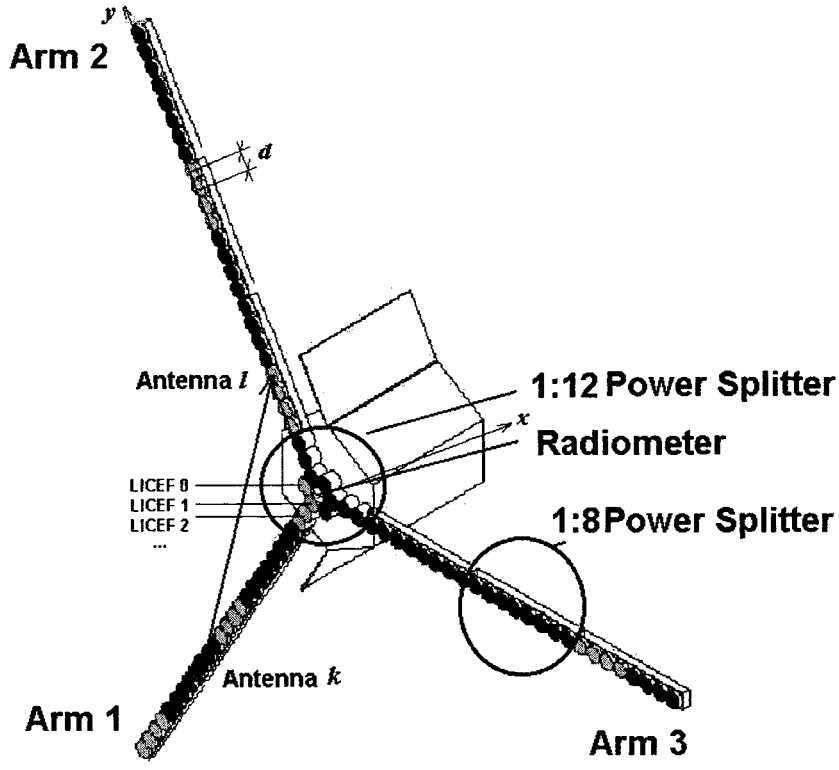

Figure 1. MIRAS Y-shaped interferometric radiometer. MIRAS Demonstrator Pilot Project configuration: 27 elements per arm space d = 0.89 wavelengths, total arm length equals 5.5195 m.

120°. In the MIRAS Demonstrator Pilot Project there are 27 *L* band dual-polarization antenna-receiver units (called Light and Cost Effective Front-Ends (LICEFs), which refers to the subsystem formed by the antenna and the receiving electronics whose output is the digital in-phase and quadrature components.) in each arm (Figure 1). This structure is compatible with a spatial resolution of 50 km and a swath of 960 km from a 672 km height Sun-synchronous orbit.

The element at the center of the array is connected to a noise injection radiometer for total power calibration and the measurement of the antenna temperature (zero baseline): $T_A = V(0,0)$. Each arm has a part in the hub fixed to the spacecraft (center circle, Figure 1) and another one, which is deployed in orbit. The fixed part of each arm consists of 4 antenna-receiver elements, one of them between the Y arms for phase calibration and redundancy in case of failure. The deployable arms comprise 3 sections of 8 elements each. The outputs of every 4 LICEFs are multiplexed by a serial optical transmitter-receiver (SOTR) and sent to the hub, to evaluate the different visibility samples (V_{kl}, Equation (1)) from the normalized ones (μ_{kl}) measured by the matrix of 1 bit / 2 level digital correlators [*Hagen and Farley*, 1973],

$$V_{kl} = \sqrt{T_A + T_{Rk}}\sqrt{T_A + T_{Rl}}\ \mu_{kl} \quad , \tag{2}$$

where $T_{Rk,l}$ are the noise temperatures of receivers k and l and T_A is the antenna temperature, assumed to be the same for all the elements (Differences between antenna temperatures are much smaller than those of $T_{Rk,l}$ have been omitted in (2). Slight differences in T_A may arise from different antenna patterns, which are minimized by proper antenna manufacturing.).

In sections 2-4 the system performance is studied in case of failure of the noise injection radiometer, of an antenna-receiver unit (LICEF), or of a 4:1 multiplexer (SOTR). First, the robustness of the calibration procedure is analyzed. Second, the system performance degradation is studied in terms of degradation of the spatial resolution, radiometric sensitivity, and accuracy. Finally, a reliability analysis is performed, and failure rates are assigned to each

electronics subsystem to achieve a total reliability of 90% in a 2-year mission.

2. Calibration Robustness in Case of Failures

Ideally, the calibration of a synthetic aperture interferometric radiometer should be performed by imaging a point source in the far field of the array at every independent pixel of the field of view (G matrix [*Ruf et al.*, 1988]). However, for large arrays (e.g., MIRAS arms 5.2 m long) this technique is not feasible in anechoic chambers, and transmissions are forbidden in a band reserved for radio astronomy and passive observations. A point source at boresight can be simulated by injecting correlated noise from a centralized source to all the receivers simultaneously. The response to out-of-boresight point sources is inferred from the measurement of the antenna voltage patterns and the fringe-wash function (Equation (1)) [*Camps et al.*, 1999]. However, a centralized noise distribution network is technologically very challenging. These considerations led to the proposal of a distributed noise injection scheme in which phase tracking is achieved with overlapping noise sources [*Torres et al.*, 1996; *Corbella et al.*, 1998]. The 27 elements of each arm plus 1 of the 3 extra elements (LICEF 0, Figure 1) form a set of 28, divided into 7 subsets of 4 elements (shaded groups of elements, Figure 1).

2.1. Impact of Failures in Phase Calibration

In this section the effect of LICEF/SOTR failure(s) in phase calibration is analyzed. The central elements of each arm a_0-a_3 receive correlated noise from the central source n_0, whose noise temperature T_0 has been measured by switching the noise injection radiometer input to n_0 [*Corbella et al.*, 2000a] (see Figure 2). For these 12 elements there are

$$\binom{12}{11} = 66$$

equations and 23 phase and quadrature unknowns, since all phases must be referred to one of them. In each arm the groups a_4-a_{11}, a_{12}-a_{19}, and a_{20}-a_{27} are driven by noise sources n_2, n_4, and n_6, respectively (noise temperatures T_2, T_4, and T_6), leading to 3 systems of 28 equations and 16 unknowns each. Phase tracking along each arm is achieved by connecting the odd noise sources, so as to form the groups a_8-a_{15} and a_{16}-a_{23} driven by noise sources n_3 and n_5 (noise temperatures T_3 and T_5). Table 1 summarizes the properties of the system of equations.

Phase tracking is kept if there are up to 3 element failures in a group of 8 elements. In this case, the number of equations

$$\binom{5}{4} = 10$$

equals that of unknowns $2(8-3)=10$. In case of failure of 4 elements or a SOTR, phase tracking is lost for the elements that are farther away in the arm. (In case of SOTR failure, phase tracking along the Y arms is still possible by means of redundant space

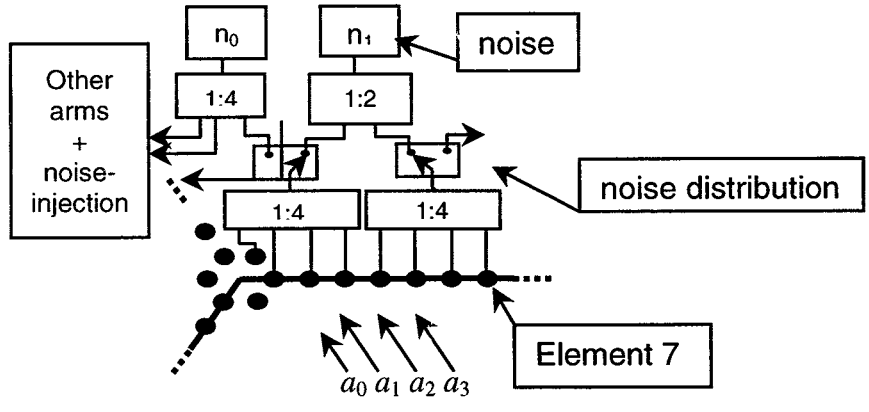

Figure 2. Diagram of the switching scheme for distributed noise injection. Noise n_0 drives the central elements, while the rest drive overlapping groups of 4 + 4 adjacent elements. In the actual implementation of MIRAS each noise source will be duplicated for redundancy [GMV, S. A., and Space Division, Construcciones Aeronáticas, S.A., 1999].

Table 1. Properties of the System of Equations for Phase Calibration

Group of Elements and Noise Source	Number of Elements	*Number of Equations*	Number of Unknowns	Comments
Central part	12	$\binom{12}{2}=66$	23	all phases are referred to an arbitrary one, set to 0.
Group a_0-a_7 (n_1)	4(+4)	$\binom{4}{2}=6,+4\text{x}4$	8	the equations of a_0-a_3 are already included in the central part; 4x4 is the number of equations from a_0-a_3 and a_4-a_7
Groups a_8-a_{15} (n_3), a_{16}-a_{23} (n_5), a_4-a_{11} (n_7), a_{12}-a_{19} (n_2), and a_{20}-a_{27} (n_4)	8	$\binom{8}{7}=28$	16	

calibration. Since the phase estimate of the baselines linking the gap of 4 receivers (> 5 x 0.89 wavelengths) is noisier than that of baseline 0.89 wavelengths, the radiometric accuracy will be degraded (*A. Camps et al.*, Redundant space calibration of hexagonal and Y-shaped radars and interferometric radiometers, submitted to *Radio Science*, 1999)).

2.2 Impact of Failures in Amplitude Calibration

The amplitude factors required to determine V_{kl} from μ_{kl} (Equation 2) are different during the measurement $(T_A+T_{Rk,l})^{1/2}$ and during the calibration $(T_{ck,l}+T_{Rk,l})^{1/2}$, where $T_{ck,l}$ is the correlated noise temperature at the receivers input. Therefore it is necessary to estimate T_A, T_{ckl} and $T_{Rk,l}$ independently. Since the measurements are performed by the noise-injection radiometer and the power detectors of each receiver, the estimation of the noise temperature of one receiver is not affected by the failure of other receivers.

3. System Performance Degradation in Case of Failures

Instrument performance is determined by three basic parameters: spatial resolution, radiometric sensitivity, and radiometric accuracy. Failure of single or multiple elements of the instrument causes a degradation of these parameters. In this section we will analyze which one is more sensitive to element failure and it will be selected to perform the reliability analysis in section 4. In the following analysis, missing visibility samples are set to 0 to avoid interpolation-induced artifacts.

3.1. Spatial Resolution

Spatial resolution is determined by the width of the equivalent array factor AF_{eq} [*Bará et al.*, 1998]. In order to gain insight into the properties of a Y array with missing elements the (u,v) spatial frequency coverage of MIRAS and the equivalent array factor with Blackmann windowing are computed for no failures, or for a LICEF/SOTR failure (Figure 3). Figure 3 shows the (u,v) points sampled by a Y array with no failures (Figure 3a), failure of LICEF 2 (second element in one arm; Figure 3b), failure of SOTR 0 (multiplexer of antennas 0-3 in one arm) (Figure 3c) and failure of SOTR 1 (multiplexer of antennas 4-7) (Figure 3d). The symmetry of Figures 3a-3d with respect to (0,0) is due to the property of the visibility function $V(-u,-v) = V^*(u,v)$. The circles marked in Figure 3a show the missing (u,v) samples when the central antenna is connected to the noise injection radiometer and it is not used to compute cross correlations with other antennas outputs. Its impact on the impulse response or equivalent array factor AF_{eq} is negligible. Figures 3e, 3f, 3g and 3h show the AF_{eq} contour plots corresponding to Figures 3a, 3b, 3c and 3d at levels 0, –3, –5, –10, –13, –15, and –20 dB, computed with Blackmann window. As can be appreciated, the shape of the main lobe does not degrade noticeably. The largest differences appear at the sidelobe level when SOTR 1 fails, for which the side lobe level rises to about –9 dB. When LICEF 2 fails the sidelobe level rises to about –13.5 dB. Numerical simulations have shown that (1) The impact of a LICEF/SOTR failure in the main beam efficiency and the half-power synthetic beam width of

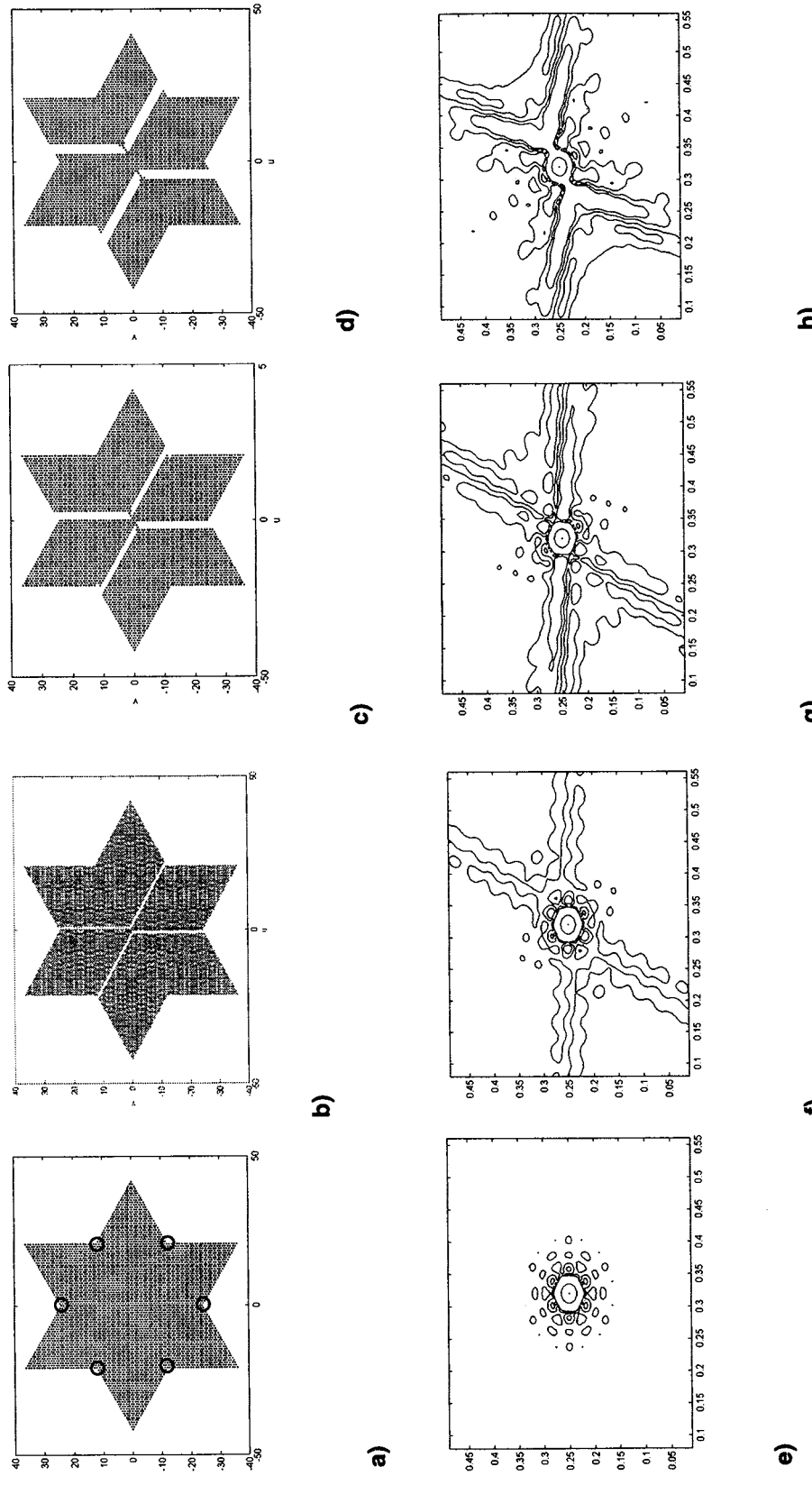

Figure 3. Spatial frequency coverage ((u,v) points) sampled by a Y array with (a) no failures, (b) failure of LICEF 2 (second element in one arm), (c) failure of SOTR 0 (multiplexer of antennas 0-3 in one arm), and (d) failure of SOTR 1 (multiplexer of antennas 4-7). Equivalent array factor contour plots at -0.04, −3, −5, −10, −13, −15, and −20 dB, corresponding to (e) Figure 3a, (f) Figure 3b, (g) Figure 3c, and (h) Figure 3d.

the AF_{eq} is always smaller than 10% (failure of LICEF 2) when compared to the ideal values (no failures) quoted by *Bará et al.* [1998]. (2) The failure of a SOTR produces a larger degradation of the equivalent array factor than that of a LICEF, since the number of missing (u,v) points is larger in the first case. (3) The failure of LICEF 1 does not impact the shape of the equivalent array factor, since it is redundant with LICEF 0, located between the Y arms and (4) The impact of a LICEF-SOTR failure decreases for LICEFs-SOTRs farther away from the center of the Y array. A single failure of LICEFs 17-27 or SOTRs 4-6 (provided phase tracking is kept) has a negligible impact on the sidelobe level.

3.2. Radiometric Sensitivity and Accuracy

The radiometric sensitivity, defined as the smallest change in the average brightness temperature that can be detected by the instrument, is given by [*Camps et al.*, 1998b]

$$\Delta T = \Omega_{eq} \frac{\sqrt{3}}{2} d^2 T_{sys} \frac{\alpha_{LO}}{\alpha_F \sqrt{B \tau_{eff}}} \sqrt{\sum_m \sum_n W_{mn}^2} \quad , \quad (3)$$

where Ω_{eq} is the antenna equivalent solid angle ($\Omega_{eq} \approx 1.60$ for a 9dB directivity), $d = 0.89$ wavelengths, $T_{sys} = T_A + T_R$ is the system's temperature, $\alpha_{LO} = 1$ or 1.41 for single side band or double side band receivers, α_f is a frequency response factor in the range 1-1.19, B is the noise-equivalent bandwidth, τ_{eff} is the effective integration time [*Hagen and Farley*, 1973], and W_{mn} is the window used to taper the spatial frequency (u_{mn}, v_{mn}). Since ,

$$\sum_m \sum_n W_{mn}^2 \Big|_{\text{no failure}} > \sum_m \sum_n W_{mn}^2 \Big|_{\text{LICEF and/or SOTR failure}} \quad (4)$$

the radiometric sensitivity in case of LICEF and/or SOTR failures is always better than in the case of no failure. This apparent paradox reaches a limit situation when all the LICEFs fail but the central one, corresponding to a constant brightness temperature estimate given by T_A. Hence the radiometric sensitivity cannot be used to assess the impact on instrument performance of single- or multiple-element failure.

The radiometric accuracy is defined as the rms systematic error between the actual (T^{id}) and the recovered (T^{rec}) brightness temperature images

$$\Delta T_{rms} = \sqrt{\frac{1}{M-1} \sum_{m=1}^{M} \left(T_m^{rec} - T_m^{id} \right)^2} \quad , \quad (5)$$

where the subscript indicates pixel number m from a total of M in the field of view. The same realistic brightness temperature image as used by *Camps et. al.* [1998a, Figure 3] has been used in order to analyze the radiometric accuracy degradation. Visibility samples have been computed numerically assuming identical antennas and receivers. To avoid the dependence of the results on any particular inversion algorithm, T^{rec} has been obtained by means of a hexagonal inverse Fourier transform weighted by rectangular or Blackmann windows with zero padding for the missing visibility samples. Simulation results are shown in Figures 4a and 4b for a single LICEF or SOTR failure, respectively. As can be appreciated, the failure of LICEFs 0 or 1 is not critical since they are redundant. The worst situation is the failure of LICEF 2 or SOTR 0, for which the radiometric accuracy degrades by 13.4 and 24.5 K, respectively. These results will be used in section 4 to assess the reliability of each subsystem.

4. Reliability Analysis of Y-shaped Interferometric Radiometers

According to section 3, the radiometric accuracy degradation is the most restrictive parameter and is selected in the reliability analysis. In addition, in order to maintain phase tracking along the Y arms the failure of a SOTR cannot be tolerated. In case of failure of a SOTR, if phase tracking is still possible, failure of SOTRs 4, 5, or 6 will produce a radiometric accuracy degradation lower than 1.9 K (Figure 4b).

In order to assure a degradation approximately smaller than 3 K (see SMOS proposal by Y. H. Kerr, available from Centre d'Etudes Spatiales de la Biosphére at http://www-sv.cict.fr/cesbio/smos/) each arm has been divided into three zones (Figure 1) according to the following criteria:

1. Zone 1 is composed of LICEFs 2-8 and the extra LICEF (not drawn). These LICEFs cannot fail since the radiometric accuracy degrades above 2.7 K (Figure 4a), except for LICEF 1, which is redundant with LICEF 0.

2. Zone 2 is composed of LICEFs 9-16. The failure of one and only one of these LICEFs degrades the radiometric accuracy below 2.7 K. So, a single failure is allowed. Actually the overall radiometric accuracy

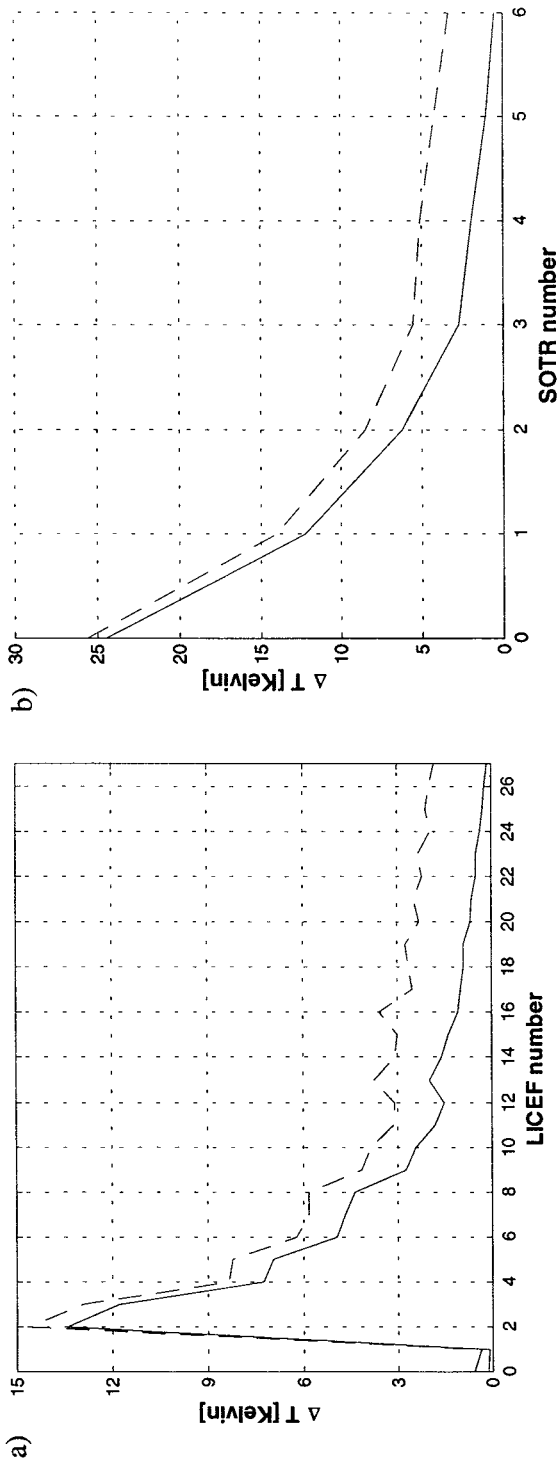

Figure 4. Degradation of the radiometric accuracy when (a) a LICEF or (b) a SOTR fails. Blackmann (solid line) and rectangular (dashed line) windows. In Figure 4b it has been assumed that phase tracking has been kept with negligible error.

must include other error sources analyzed in previous works [*Torres et al.*, 1997; *Camps et al.*, 1997a,1997b]. Table 1 in *Corbella et al.* [2000b], summarizes the radiometric accuracy error budget. In case of no failure, ΔT = 1.8 K; in case of failure of LICEF 9, $\Delta T = ((2.7\ \mathrm{K})^2 + (1.8\ \mathrm{K})^2)^{1/2} = 3.2$ K; in case of failure of LICEF 10, ΔT = 3.1 K, in case of failure of LICEF 11, ΔT = 2.7 K, etc. Nevertheless, the failure of two LICEFs in any position of zone 2, even in different arms is not tolerable.

3. Finally, zone 3 consists of LICEFs 17-27. Up to two simultaneous failures in the same arm, and up to three simultaneous failures in different arms, can be tolerated with a radiometric accuracy degradation smaller than 2.7 K.

The simultaneous failure of two LICEFs in different zones results in unacceptable radiometric accuracy degradation.

In this reliability analysis the following assumptions have been performed: (1) Two cases have been considered: The subsystem operates properly or it fails. (2) The failure of any subsystem (noise injection radiometer, LICEF, and/or SOTR) can be detected, through an anomalous brightness temperature or correlation product(s). (3) The probability of operation associated with a working time t or reliability function is assumed to be exponential $R(t) = \exp(-\lambda t)$ (maturity period of a piece of electronic equipment) with a failure rate of λ failures per year. (4) All LICEFs and all SOTRs have the same reliability function's $R_{LICEF}(t)$ and $R_{SOTR}(t)$, respectively.

The goal is to guarantee a radiometric accuracy degradation smaller than 3 K, ensuring the quality of the calibration process in a 2-year mission. Since the reliability functions of the noise injection radiometer ($R_1(t)$), the set of 21 SOTRs ($R_2(t)$), and the set of 84 LICEFs ($R_3(t)$) are independent, the reliability function of the total system is

$$R_{\mathrm{total}}(t) = R_1(t)\, R_2(t)\, R_3(t)\,. \qquad (6)$$

The computation of $R_1(t)$, $R_2(t)$, and $R_3(t)$ is detailed in Appendix 1. If (1) the global reliability is set to 90% at the end of a two-year mission, (2) there is no redundancy, and (3) the reliability is evenly distributed ($R_1(t) = R_2(t) = R_3(t) = \sqrt[3]{0.9} = 0.9655$), the reliability functions (R_{NIR}, R_{SOTR}, and R_{LICEF}) and failure rates (λ_{NIR}, λ_{SOTR}, and λ_{LICEF}) associated with the noise injection radiometer, the SOTRs, and the LICEFs can be derived from (A1), (A2) and (A16):

Table 2. Reliability and Failure Rate of Each SOTR Versus the Number of Redundant Elements for a 96.55% Reliability (90% Global Reliability).[a]

Number of Redundant SOTRs	SOTR's Reliability R_{SOTR}	Failure Rate λ_{SOTR}, 10^{-4} failures/y
0	0.9983	8.4
1	0.9981	9.8
2	0.9977	12
3	0.9971	15
4	0.9961	19
5	0.9942	29
6	0.9891	55
7	0.9591	209

[a] The first row shows the MIRAS configuration (no redundancy). Redundant SOTRs are placed beginning at the center of the Y-array

$R_{NIR} = 0.9655$, $R_{SOTR} = 0.9983$, $R_{LICEF} = 0.9984$, $\lambda_{NIR} = 175.6 \times 10^{-4}$, $\lambda_{SOTR} = 8.4 \times 10^{-4}$, $\lambda_{LICEF} = 7.8 \times 10^{-4}$ failures/y.

Tables 2 and 3 summarize the reliability and failure rates of the SOTRs and LICEFs, respectively, for a global reliability of 90% after 2 years, as a function of the number of redundant elements, placed starting at the center of the array. An examination of these values shows the trade-off between increased system complexity and subsystem reliability. A good compromise may be the duplication of all the SOTRs and LICEFs 1-11 in each arm (those of the central part and those in the first section of the arms). In this case their failure rate is required to be $\lambda_{SOTR} = 209 \times 10^{-4}$ and $\lambda_{LICEF} = 76 \times 10^{-4}$ failures/y.

5. Conclusions

This paper has analyzed the reliability of Y-shaped synthetic aperture interferometric radiometers at the subsystem level. To do this, system performance degradation has been first studied in terms of spatial resolution, radiometric sensitivity, and radiometric accuracy in case of failure of the elements (LICEFs), the multiplexers (SOTRs), and/or the noise injection radiometer. The following points have been shown: (1) The shape of the main beam of the impulse response is not significantly modified. The half-power width of the synthetic beam is almost unaffected, and therefore the spatial resolution is almost unaffected. The sidelobe level increases, and the main beam efficiency is always degraded less than 10% of its

Table 3. Reliability and Failure Rate of Each LICEF Versus the Number of Redundant Elements for a 96.55% Reliability (90% Global Reliability).[a]

Number of Redundant SOTRs	SOTR's Reliability R_{SOTR}	Failure Rate λ_{SOTR}, 10^{-4} failures/y
0	0.9986	6.9
1	0.9984	7.8
2	0.9982	8.9
3	0.9979	10
4	0.9976	12
5	0.9971	15
6	0.9963	18
7	0.9953	24
8	0.9938	31
9	0.9917	42
10	0.9888	57
11	0.9849	76
12	0.9798	102

[a] The second row shows the MIRAS configuration (one redundant LICEF located between the *Y* arms). Other redundant LICEFs may be located duplicating each *Y* arm. Redundant LICEFs are placed beginning at the center of the *Y* arms.

nominal value (failure of LICEF 2) in case of no failures. (2) The radiometric sensitivity is mostly unaffected. (3) The radiometric accuracy is seriously degraded in case of failure of an element and/or a multiplexer. This degradation is more important for the elements and/or multiplexers closest to the center of the array; for example, for failure of LICEF 2 the radiometric accuracy degradation is 13.4 K. (4) From point 3, redundant elements and/or multiplexers must be placed along the arms beginning from the center of the Y array.

Assuming a worst case 3.2 K radiometric accuracy (ΔT= 1.8 K for an instrument without failures and $\Delta T = 3.2\,\mathrm{K} = \sqrt{(2.7\,\mathrm{K})^2 + (1.8\,\mathrm{K})^2}$ in case of failure of LICEF 9) and redundancy in all the multiplexers and elements 1-11 (elements 0 and 1 are already redundant), for a 90% reliability in a 2-year mission, the failure rate of the noise injection radiometer, the multiplexers, and the elements is required to be approximately $\lambda_{NIR} \approx 1.8 \times 10^{-2}$, $\lambda_{SOTR} \approx 2.1 \times 10^{-2}$ and $\lambda_{LICEF} \approx 0.76 \times 10^{-2}$ failures/y, respectively.

Appendix A: Analysis of Subsystem Reliability Functions

A1. Reliability Function of the Noise Injection Radiometer (NIR)

If the noise injection radiometer fails, the baseline $V(0,0)$ and the absolute scale are lost (T_A and the amplitude factors in Equation 2). Since there is only one radiometer, the associated reliability function is

$$R_1(t) = (1-p)^1 = R_{NIR}(t) \qquad \text{(A1)}$$

where p is the probability of failure of each unit. For simplicity, it is assumed that the probability of failure p is the same for the NIR, the SOTRs, and the LICEFs.

A2. Reliability Function of the Multiplexers

Since no SOTR failure can be tolerated the reliability function is

$$R2(t) = (1-p)^{21} = R_{SOTR}^{21}(t) \qquad \text{(A2)}$$

A3. Reliability Function of the Antennas-Receivers

The maximum number of LICEFs (including the ones between the Y arms) that can fail simultaneously is 7. Hence the probability of a radiometric accuracy degradation smaller than 3 K is

$$P = \sum_{x=0}^{7} p_r(x,84,p) \quad , \qquad \text{(A3)}$$

where x is the number of failures, 84 is the total number of units (84 different LICEFs), and p is the probability of failure of each unit. The probability $p_r(x,84,p)$ depends on the position of each LICEF. Each probability $p_r(x,84,p)$ in (A3) is computed as follows [*Gómez and Canela*, 1994]:

1. The probability of no failures at all is

$$p_r(0,84,p) = (1-p)^{84} \quad . \qquad \text{(A4)}$$

2. The probability of one acceptable failure is

$$p_r(1,84,p) = p(1-p)^{83}(a_1 + r_1) \quad , \qquad \text{(A5)}$$

where $a_1 = 3\ X_{100}$ is the total number of LICEF combinations that can produce one failure in the second and third zones, in any of the three arms, X_{100} = 19 is the number of LICEF combinations that produce one failure in one arm (LICEFs 9-27) and 0 failures in the other two arms, and $r_1 = 6$ is the total number of redundant LICEFs combinations that can produce an individual failure in the first zone (LICEFs 0 and 1 of any arm). Finally,

$$p_r(1,84,p) = 63p(1-p)^{83} \quad . \qquad \text{(A6)}$$

3. The probability of two acceptable failures is

$$p_r(2,84,p) = p^2(1-p)^{82}(a_2 + a_1 r_1 + r_2) \quad , \qquad \text{(A.7)}$$

where $a_2 = 3\ X_{110} + 3\ X_{200} = 528$ is the total number of LICEFs combination that can produce two simultaneous failures in the second and third zones in any of the three arms, X_{110} = 11 x 11 = 121 is the number of LICEF combinations that produce one failure in two arms and zero failures in one arm (LICEFs 17-27), X_{200} = 11 x 10/2! = 55 is the number of LICEF combinations that produce two failures in one arm (third region) and zero in the other two arms, and r_2 = 12 is the number of combinations of redundant LICEFs that produce two simultaneous failures in the first zone that do not affect system performance: failure of LICEF 1 of one arm and LICEF 0 of another arm. Finally,

$$p_r(2,84,p) = 882p^2(1-p)^{82} \quad . \qquad \text{(A8)}$$

4. The probability of three acceptable failures is

$$p_r(3,84,p) = p^3(1-p)^{81}\left(a_3 + a_2 r_1 + a_1 r_2 + r_3\right) \quad , \tag{A9}$$

where: $a_3 = X_{111} + 6X_{210} + 3X_{300} = 5456$ is the total number of LICEFs combination that can produce three simultaneous failures one in each arm (X_{111}), two in one arm and another in a second arm (X_{210}) or three in a single arm (X_{300}); $X_{111} = 11^3 = 1331$, $X_{210} = (11 \times 10/2) \times 11 = 605$ and $X_{300} = 11 \times 10 \times 9/3! = 165$, since these failures can only be tolerated in the third zone; and $r_3 = 8$ is the number of combinations of redundant LICEFs that produce three simultaneous failures. Finally,

$$pr(3,84,p) = 9316p^3(1-p)^{81} \quad . \tag{A10}$$

5. The probability of four acceptable failures is

$$p_r(4,84,p) = p^4(1-p)^{80}\left(a_4 + a_3 r_1 + a_2 r_2 + a_1 r_3\right) \quad , \tag{A11}$$

where $a_4 = 3X_{211} + 3X_{220} + 6X_{310} = 39930$ is the total number of LICEFs combination that can produce two simultaneous failures in one arm and one in the other two arms (X_{211}), two failures in two arms and zero in the third arm (X_{220}), and three failures in one arm and one in another arm (X_{310}) and $X_{211} = (11 \times 10/2) \times 11^2 = 6655$, $X_{220} = (11 \times 10/2)^2 = 3025$, and $X_{310} = (11 \times 10 \times 9/3!) \times 11 = 1815$, since these failures can only be tolerated in the third zone. Finally,

$$p_r(4,84,p) = 79{,}458\,p^4(1-p)^{80} \quad . \tag{A12}$$

In a similar way, the probability of five, six and seven acceptable failures is not zero because of the three redundant LICEFs (a_5, a_6, $a_7 = 0$):

$$p_r(5,84,p) = p^5(1-p)^{79}\left(a_4 r_1 + a_3 r_2 + a_2 r_3\right) = 309{,}276\,p^5(1-p)^{79} \tag{A13}$$

$$pr(6,84,p) = p^6(1-p)^{78}\left(a_4 r_2 + a_3 r_3\right) = 522{,}808\,p^6(1-p)^{78} \quad , \tag{A14}$$

$$p_r(7,84,p) = p^7(1-p)^{77}\left(a_4 r_3\right) = 319{,}440\,p^7(1-p)^{77} . \tag{A15}$$

Substituting (A4), (A6), (A8), (A10), (A13), (A14), and (A15) into (A3), the reliability function associated to the set of LICEFs ($R_3(t)$) can be computed as

$$R_3(t) = \sum_{i=0}^{7} m_i (1 - R_{\mathrm{LICEF}})^i R_{\mathrm{LICEF}}^{84-i} \quad , \tag{A16}$$

where the fators $m_0 = 1$, $m_1 = 63$, $m_2 = 882$, $m_3 = 9316$, $m_4 = 79{,}458$, $m_5 = 309{,}276$, $m_6 = 522{,}808$, and $m_7 = 319{,}440$ have been derived previously. Finally, the total reliability function is obtained substituting (A1), (A2) and (A16) in (6).

Acknowledgments. This work has been performed under ESA contract "MIRAS Failure Analysis" (FAN; TOS-ETP/055.98/MMN), and the Spanish Comisión Interministerial de Ciencia y Tecnologia (CICYT TIC99-1050-C03-01). The authors would like to express their gratitude to an anonymous reviewer for his/her comments and suggestions in improving the completeness and clarity of the manuscript.

References

Bará, J., A. Camps, F. Torres, and I. Corbella, Angular resolution of two-dimensional hexagonally sampled interferometric radiometer, Radio Sci., 33 (5), 1459-1473, 1998.

Camps, A., J. Bará, I. Corbella, and F. Torres, The processing of hexagonally sampled signals with standard rectangular techniques: Application to 2D large aperture synthesis interferometric radiometers, IEEE Trans. on Geosci. Remote Sens., GRS-35 (1), 183-190, 1997a.

Camps, A., J. Bará, F. Torres, I. Corbella, and J. Romeu, Impact of antenna errors on the radiometric accuracy of large aperture synthesis radiometers: Study applied to MIRAS, Radio Sci., 32 (2), 657-668, 1997b.

Camps, A., J. Bará, F. Torres, and I. Corbella, Extension of the CLEAN technique to the microwave imaging of continuous thermal sources by means of aperture synthesis radiometers, paper presented at Progress In Electromagnetics Research, Symposium 1998 (PIER 18), Electromagn. Acado, University of Washington, Seattle, USA, Jan. 1998a.

Camps, A., I. Corbella, J. Bará, and F. Torres, Radiometric sensitivity computation in aperture synthesis interferometric radiometry, IEEE Trans. Geosci. Remote Sens., GRS-36, (2), 680-685, 1998b. (Correction, IEEE Trans. Geosci. Remote Sens., *GRS-36* (5), 1835, Sept. 1998).

Camps, A., F. Torres, J. Bará, I. Corbella, and F. Monzón, Automatic calibration of channels frequency response in interferometric radiometers, Electron. Lett., 35 (2), 115-116, 1999.

Corbella, I., F. Torres, A. Camps, and J. Bará, A new calibration technique for interferometric radiometers,

paper presented at the European Symposium on Aerospace Remote Sensing, Conference on Sensors, Systems and Next Generation Satellites IV (EUROPTO), sponsored by EOS-SPIE-NASA, Barcelona, Spain, Sept. 1998.

Corbella, I., A. Camps, F. Torres, and J. Bará, Analysis of noise-injection networks for interferometric-radiometer calibration, *IEEE Trans. Microwave Theory Tech.*, 48 (4), 545-552, 2000.

Corbella, I., F. Torres, A. Camps, J. Bará, N. Duffo, and M. Vall.llossera, *L*-band aperture synthesis radiometry: hardware requirements and system performance, paper presented at International Geoscience and Remote Sensing Symposium IGARSS 2000, Honolulu, Hawaii, July 24-28, 2000b.

GMV, S.A. and Space Division, Construcciones Aeronáticas, S.A., Technical note on soil moisture and ocean salinity parametric mission design: MIRAS, MPD-GMV-10100-TN0-001, Madrid, 1999.

Gómez, G., and M. A. Canela, Fiabilitat industrial, Edicions UPC, pp. 97-108, 1994.

Hagen J. B., and D. T. Farley, Digital-correlation techniques in radio science, *Radio Sci.*, 8 (8-9), 775-784, 1973.

Ruf, C.S., C. T Swift, A. B. Tanner, and D. M. LeVine, Interferometric synthetic aperture radiometry for the remote sensing of the Earth, *IEEE Trans. Geosci. Remote Sens.*, 26 (5), 597-611, 1988.

Thompson, A. R., J. M. Moran, and G. W. Swenson, *Interferometry and Synthesis in Radio Astronomy*, John Wiley, New York 1986.

Torres, F., A. Camps, J. Bará, I. Corbella and R. Ferrero, On-board phase and modulus calibration of large aperture synthesis radiometers: Study applied to MIRAS, *IEEE Trans. on Geosci. Remote Sens.* GRS-34 (4), 1000-1009, 1996.

Torres, F., A. Camps, J. Bará, and I. Corbella, Impact of receiver errors on the radiometric resolution of large 2D aperture synthesis radiometers: Study applied to MIRAS, *Radio Sci.*, 32 (2), 629-642, 1997.

J. Bará, A. Camps, I. Corbella, N. Duffo, F. Torres and M. Vall-llossera, Universitat Politècnica de Catalunya, Campus Nord UPC D3, Jordi Girona 1-3, 08034 Barcelona, Spain. (merce@tsc.upc.es)

(Received June 23, 2000; revised September 27, 2000; accepted October 2, 2000.)